AEGC2019 Data to Discovery
Australasian Exploration Geoscience Conference
2-5 September 2019 • Perth, Western Australia
Incorporating the AIG, ASEG, PESA, and WABS

Understanding the causes of low frequency shadow below gas hydrates

Ayman Noor M. Qadrouh*
King Abdulaziz City for Science and Technology (KACST)
aqadrouh@kacst.edu.sa

Saad Alajmi
King Abdulaziz City for Science and Technology (KACST)
aqadrouh@kacst.edu.sa

SUMMARY

Gas hydrates consider as one of the prospective natural resource that can supply energy. The seismic method has successfully been applied to locate gas hydrates. Their presence is revealed by bottom simulating reflectors (BSR) which represent the seismic signature of the base of gas-hydrate saturated sediments, with a layer partially saturated with free gas below the BSR. It is observed that the seismic response of the BSR is characterized by low frequency, which it is called the low frequency shadow (LFS). The possible causes of LFS are the presence of free gas or normal moveout (NMO) stretching. In order to have a deep understanding of the low frequency shadow causes, 1D and 2D synthetic seismograms and spectrograms are computed. The 1D and 2D simulations of seismic signal are based on rock physics and numerical modelling, considered the effect of the seismic attenuation and NMO stretch. The results of numerical seismograms and spectrograms show that attenuation affects the lower interface with minimum amplitudes for lower values. The quantification of the maximum frequency is obtained as the shift of the centroid spectrum. Moreover, the non-stretch NMO corrections improve the resolution to detect the BSR layer, and a stacked trace can be achieved without loss of frequencies. As a result, using an appropriate rock physics method is required to obtain valuable knowledge about the effect of the different parameters on the wave properties.

Key words: bottom simulating reflectors (BSR), low frequency shadow (LFS), seismic attenuation and normal moveout (NMO).

INTRODUCTION

Given the increasing energy consumption and the need for alternative sources of energy, scientists have focused on unconventional energy sources such as gas hydrates (Kvenvolden, 1993; Makogon, 2010). Vast amount of methane is trapped in gas hydrates at depths of around 2000 m, where the optimal pressure and temperature conditions are 1 atm and 20°C respectively.

Seismic methods have been extensively applied to detecting gas hydrates based on the interpretation of bottom simulating reflectors (BSRs), where the BSR on seismic data is represented by the base of the gas-hydrate-bearing formation with a layer partially saturated with free gas below the BSR (Sheriff, 2002; Carcione and Gei, 2004). It is observed that the seismic response of the BSR is characterized by low frequencies, called the low-frequency shadow (LFS) (Taylor et al., 2000). The frequency content depends on the offset, with the BSR response having a lower dominant frequency at large offsets. The common interpretation for the shift toward lower frequency below the BSR is mesoscopic-loss effects because of the presence of gas (e.g. Carcione and Picotti, 2006; Qadrouh et al., 2015; Qadrouh et al., 2016). The LFS phenomena not only appears below the BSR, but it also can be seen in seismic exploration of hydrocarbons that correspond to bright spots (Castagna et al., 2003; Ebrom, 2004; Wang et al., 2014). The LFS is normally used to indicate directly the location of the hydrocarbons (Taner et al., 1979). However, according to Barnes (2013), only a few examples of LFSs are convincing to reveal the presence of gas.

For several years great effort has been devoted to the study of low frequency shadow causes. Castagna et al. (2003) showed that at lower frequencies, the shadow is stronger compared to the reflection of reservoir. They suggested that the low frequency shadow is not solely due to seismic attenuation as the energy of low frequency could be added or amplified physically or numerically. In addition, they mentioned that the attenuation gradually decreases the high frequency, rather than cause an abrupt shift from high to low frequencies. Moreover, Castagna et al. (2003) put forward other mechanisms that can explain the occurrence of low frequency shadow such as intrinsic attenuation, peg-leg multiples, deconvolution and normal moveout (NMO) stretching at far offset. In addition, Ebrom (2004) attributed the cause of low frequency shadow to stack-related and other mechanisms. He proposed ten mechanisms that could lead to the occurrence of low frequency shadow, and these mechanisms may decrease the actual frequency by mis-stacking. In fact, based on the review of related literature, there is no consensus on the causes of low frequency shadow. Moreover, only few examples of low-frequency shadows convincingly reveal the presence of gas (Barnes, 2013).

In this study, we intend to investigate the effects caused by seismic attenuation and normal moveout stretching. In order to have a deep understanding of the low frequency shadow causes, 1D and 2D synthetic seismograms and spectrograms are computed. The 1D and 2D simulations of seismic signal are based on rock physics and numerical modelling.

METHOD AND RESULTS

In order to study this phenomena, 1D and 2D synthetic seismograms are computed by assuming a high-loss BSR layer and varying the quality factor and thickness of the layer. First, the shift of the centroid frequency of the power spectrum is estimated as a function of the travelled distance. Then, 1D experiments perform to quantify the frequency loss in seismic events below the BSR as function of the Q factor of the BSR layer and layer thickness (wave interference). Then, shot gathers are computed and then performing the standard

seismic data processing sequence to obtain the stacked section, with and without the NMO-stretch correction in the BSR layer. In all these cases, the intensity of the LFS is evaluated.

The media are described by a poroelastic model based on a generalisation of Gassmann equation. In particular, the upper medium containing gas hydrates is a sediment whose skeleton has three phase, namely, quartz, clay and gas hydrate, forming three frames. The model also describes the BSR layer partially saturated with gas as a particular case. The modelling algorithm is based on a spectrum of relaxation mechanisms and the differential equations are solved in the space-time domain by using a direct method based on the Fourier pseudospectral method.

A 1D model the LFS below the BSR is analysed, i.e. the waveform and spectrum of the BSR event and those of the lower interface. Figure 1 shows 1D simulations for different Q values and thicknesses of the BSR layer. The source dominant frequency is 25 Hz. The BSR and lower-interface events can be observed at onset times of 0.34 s and 0.65 s, approximately. The amplitude of the BSR event is maximum at h = 10 m. For h = 10 m, the BSR is one single event while it is composed of two events for h = 60 m. Attenuation affects the lower interface with minimum amplitudes for Q = 5. The importance of considering attenuation is evident, where the response of the lower interface of the BSR layer is highly attenuated (compare the dotted curves of Figures 1b and 1c).

A spectrogram for the seismic trace can be computed by using the wavelet transform (Torrence and Compo, 1998). Figure 2 shows spectrograms computed with the wavelet transform, where h denotes the thickness of the BSR layer and Q its quality factor. The vertical line indicates the location of the event reflected from the interface below the BSR layer, while the wider event, between 0.3 and 0.6 s, is the BSR response. The maximum frequency loss can be quantified as the shift of the centroid spectrum, approximately from 23 to 14 Hz, which occurs for the thicker layer. The effect is not observable for a thickness of 10 m.

A 2D CMP gather for a source dominant frequency f_p= 25 Hz is displayed in Figure 3a, where the thickness of the BSR layer is 30 m. The events at 1.2 s and 2 s correspond to the reflection events of the ocean bottom and lower interface, respectively, while the red curves in Figure 3b represent the exact traveltimes of the events reflected at the top and bottom of the BSR layer (Qadrouh et al., 2014). Figure 3c shows the difference seismograms between that of Figure 3a and one computed by considering Q = 100 in the BSR layer. The differences are substantial.

At large offsets, conventional NMO yields significantly stretched events, affecting the frequency content of the data. To avoid this artificial, the non-stretch NMO method (NSNMO) proposed by Perroud and Tygel (2004) is applied. Figure 4a shows the NMO corrected CMP gather with the conventional method, using a stretch limit large enough to include as much traces as possible in the stacked section. The quality factor of the BSR layer is 100 in this example. A semblance map is obtained for every sample, in a velocity range between 1 and 3 km/s as shown in Figure 4b. A stretch limit of 30% has been applied so the velocity analysis is conducted with limited aperture, in the validity range of the reflection-time hyperbolic approximation. According to the non-stretch NMO method, the time-velocity function is adjusted to closely follow the shape of semblance peaks, with decreasing NMO velocity along the signal pulse for each event. The conventional (green curve) and non-stretch NMO (red curve) time-velocity functions are shown in the middle panel, overlying the semblance map. They closely match the semblance peaks corresponding to the primary P reflection events. Finally, the NMO correction is applied by using the adjusted time-velocity function as shown in Figure 4c. The primary P events appear free of stretch, and correctly flattened, so a stacked trace can be correctly obtained, without loss of frequencies.

CONCLUSIONS

The seismic response of a bottom-simulating reflector are analyzed to identify the cause of the low-frequency shadow. The two most important causes are intrinsic attenuation below the BSR event (due to partial gas saturation) and NMO stretch. The main concern is the following: if frequency is lost due to intrinsic attenuation, all the events below the BSR should have decreasing dominant frequencies as a function of depth, otherwise a single low-frequency event has to be due to NMO-stretch or a similar cause. The results of 2D spectrograms show that the maximum frequency loss is quantified as the shift of the centroid spectrum which occurs for the thicker layer. Therefore, based on the rock-physics model, the shift is attributed to the presence of fluids since wave-induced fluid flow can cause attenuation. The results of NSNMO indicated that the primary reflections appear free of stretch and correctly flattened, thus correctly obtaining a stacked trace without loss of frequency. In addition, the events shapes were preserved, and each interface was easily identified. Therefore, the frequency content is preserved when NSNMO is applied.

ACKNOWLEDGEMENTS

The authors wish to thank King Abdulaziz City for Science and Technology (KACST) for funding support. We would like to extend our thanks to Prof. Jose M. Carcione for valuable discussions and sharing his experiences and knowledge.

REFERENCES

Barnes, A. E., 2013. The myth of low-frequency shadows, EAGE Workshop on Seismic Attenuation. DOI. 10.3997/2214-4609.20131834.

Carcione, J. M., Gei, D., 2004. Gas hydrate concentration estimated from P- and S-wave velocities at the Mallik 2L-38 research well, Mackenzie Delta, Canada. Journal of Applied Geophysics, 56, 73-78.

Carcione, J. M., Picotti, S., 2006. P-wave seismic attenuation by slow-wave diffusion effects of inhomogeneous rock properties. Geophysics, 71, 1-8.

Castagna, J. P., Sun, S. J., Siegfried, R. W., 2003. Instantaneous spectral analysis: detection of low-frequency shadows associated with hydrocarbons. The Leading Edge, 2, 120-127.

Ebrom, D., 2004. The low-frequency gas shadow on seismic sections. The Leading Edge, 8, 772.

Kvenvolden, K. A., 1993, Gas hydrates- geological perspective and global change. The American Geophysical Union, 31, 173-187.

Makogon, Y. F., 2010. Natural gas hydrates - A promising source of energy. Journal of Natural Gas Science and Engineering, 2, 49-59.

Perroud, H., Tygel, M., 2004. Nonstretch NMO. Geophysics, 69, 599-607.

Qadrouh, A. N., Carcione, J. M., Botelho, M. A. B., Harith, Z. Z. T., Salim, A. M., 2014. On optimal NMO and generalised Dix equations for velocity determination and depth conversion. Journal of Applied Geophysics, 101, 136-141.

Qadrouh, A. N., Carcione, J. M., Salim, A. M. A., Harith, Z. Z. T., 2016. Seismic spectrograms of an anelastic layer with different source-receivers configurations. Arabian Journal of Geoscience, 9, 1-9.

Qadrouh, A., Carcione, J. M., Salim, A. M., Harith, Z. Z. T., 2015. Attenuation effects on the seismic response of a bottom-simulating reflector. Journal of Natural Gas Science and Engineering, 24, 510-517.

Sheriff, R, E 2002. Encyclopedic Dictionary of Applied Geophysics. Society of Exploration Geophysicists, Tulsa.

Taner, M. T., Koehler, F., Sheriff, R. E., 1979. Complex seismic trace analysis. Geophysics, 44, 1041-1063.

Taylor, M. H., Dillon, W. P., Pecher, I. A., 2000. Trapping and migration of methane associated with the gas hydrate stability zone at the Blake Ridge Diapir: new insights from seismic data. Marine Geology, 164, 79-89.

Torrence, C., Compo, G. P., 1998. A practical guide to wavelet analysis. Bulletin of American Meteorological Society, 79, 61-78.

Wang, L., Gao, J., Xua, Z., Wengd, B., Jiang, X., 2014. Hydrocarbon detection using adaptively selected spectrum attenuation. Journal of Applied Geophysics, 105, 59-66.

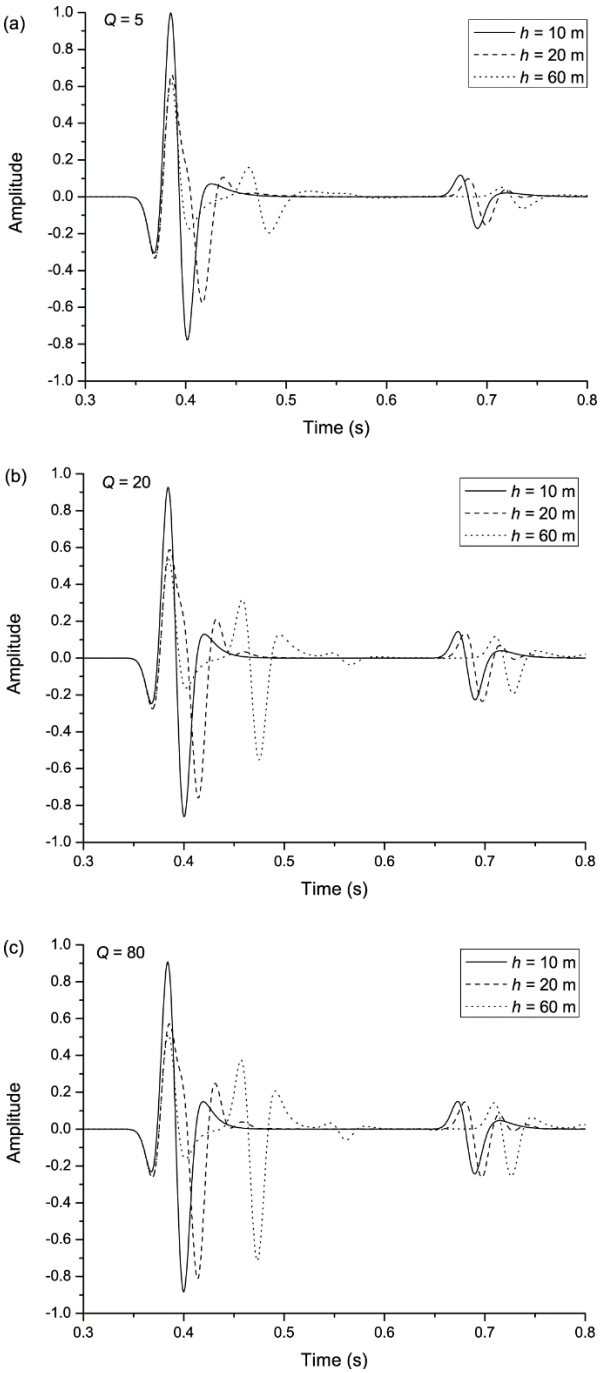

Figure 1. 1D seismic traces with different thicknesses of BSR layer and different values of quality factors.

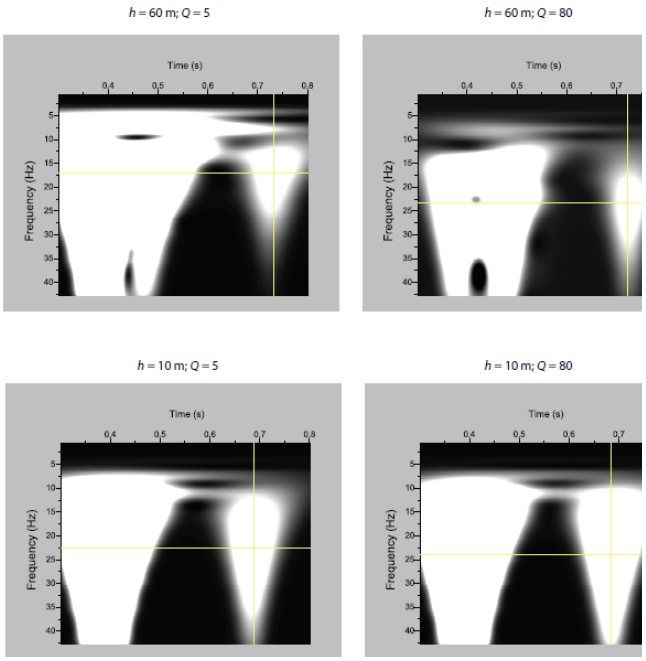

Figure 2. 2D spectrograms with different thicknesses of BSR layer and different values of quality factors.

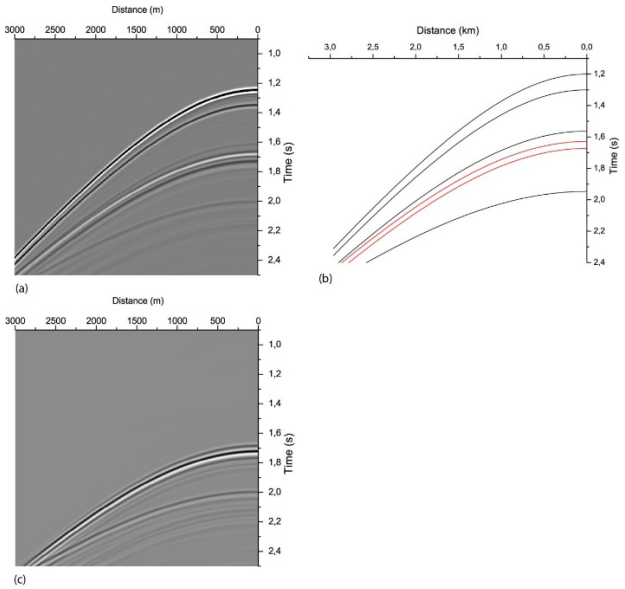

Figure 3. (a) CMP gather for Q=5, (b) exact traveltimes and (c) CMP gather for Q=100.

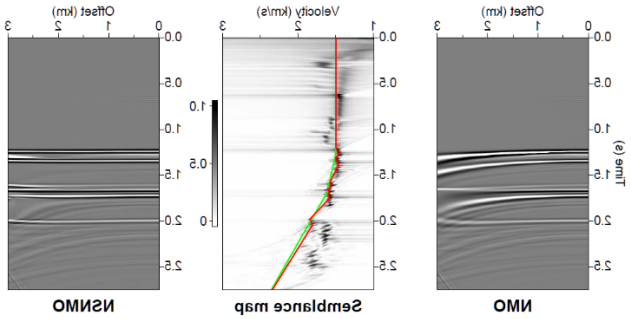

Figure 4. (a) CMP gather after conventional normal moveout corrections (NMO), (b) the green curve represents the conventional NMO while the red curve represents non-stretching normal moveout method (NSNMO), and (c) CMP gather after NSNMO.